required to retrieve the true myocardial activity concentration when compared against the in vitro ^{99m}Tc activity concentration measured from the excised myocardium.

AKNOWLEDGMENTS

This work was supported by National Cancer Institute grant 2 R01 CA50539 and by an American Heart Association Grant-in-Aid. We gratefully acknowledge financial support from the Whitaker Foundation. This work also was performed under the tenure of an Established Investigatorship from the American Heart Association for B.H. Hasegawa. We are grateful for an equipment loan from GE Medical Systems, Milwaukee, WI.

REFERENCES

1. Rosenthal MS, Cullom J, Hawkins W, Moore SC, Tsui BMW, Yester M. Quantitative SPECT imaging. A review and recommendations by the focus committee of the Society of Nuclear Medicine computer and instrumentation council. *J Nucl Med* 1995;36:1489–1513.
2. Tsui B, Frey E, Zhao X, Lalush D, Johnston R, McCartney H. The importance and implementation of accurate three-dimensional compensation methods for quantitative SPECT. *Phys Med Biol* 1994;39:509–530.
3. Kramer EL, Noz ME, Sanger JJ, Megibow AJ, Maguire GQ. CT-SPECT fusion to correlate radiolabeled monoclonal antibody uptake with abdominal CT findings. *Radiology* 1989;172:861–865.
4. Turkington TG, Jaszczak RJ, Pelizzari CA, Harrison CC, MacFall JR, Hoffman JM. Accuracy of registration of PET, SPECT and MR images of a brain phantom. *J Nucl Med* 1993;34:1587–1594.
5. Lang TF, Hasegawa BH, Liew SC, Brown JK, Blankespoor SC, Reilly SM. Description of a prototype emission-transmission CT imaging system. *J Nucl Med* 1992;33:1881–1887.
6. Hasegawa BH, Brown JK, Lang TF, Reilly SM, Liew SC, Gingold EL. Object-specific attenuation correction of SPECT with simultaneous x-ray CT. *IEEE Trans Nucl Sci* 1993;40:1242–1252.
7. Kalki K, Heanue JA, Blankespoor SC, Wu X, Brown JK, Cann CE. A combined SPECT and CT medical imaging system. *Proc SPIE* 1995;2432:367–375.
8. Hasegawa BH, Stebler B, Rutt BK, Martinez A, Gingold EL, Barker C. A prototype high-purity germanium detector system with fast photon-counting circuitry for medical imaging. *Med Phys* 1991;18:900–909.
9. Shepp LA, Vardi Y. Maximum likelihood reconstruction for emission tomography. *IEEE Trans Med Imag* 1982;MI-1:113–122.
10. Lange K, Carson R. EM reconstruction algorithms for emission and transmission tomography. *J Comput Assist Tomogr* 1984;8:306–316.
11. Kessler RM, Ellis JR, Eden M. Analysis of emission tomographic scan data: limitations imposed by resolution and background. *J Comput Assist Tomogr* 1984;8: 514–522.
12. LaCroix KJ, Tsui BMW, Hasegawa BH, Brown JK. Investigation of the use of x-ray CT images for attenuation correction in SPECT. *IEEE Trans Nucl Sci* 1994;41:2793–2799.
13. Tsui BMW, Gullberg GT, Edgerton ER, Ballard JG, Perry JR, McCartney WH. Correction of nonuniform attenuation in cardiac SPECT imaging. *J Nucl Med* 1989;30:497–507.
14. Li J, Jaszczak RJ, Greer KL, Gilland DR, DeLong DM, Coleman RE. Evaluation of SPECT quantification of radiopharmaceutical distribution in canine myocardium. *J Nucl Med* 1995;36:278–286.
15. Bartlett ML, Bacharach SL, Voipio-Pulkki LM, Dilsizian V. Artifactual inhomogeneities in myocaridal PET and SPECT scans in normal subjects. *J Nucl Med* 1995;36: 188–195.
16. Jaszczak RJ, Greer KL, Floyd CE. Improved SPECT quantification using compensation for scattered photons. *J Nucl Med* 1984;25:893–900.
17. Tung CH, Gullberg GT. A simulation of emission and transmission noise propagation in cardiac SPECT imaging with nonuniform attenuation correction. *Med Phys* 1993;21:1565–1576.
18. Liew SC, Hasegawa BH, Brown JK, Lang TF. Noise propagation in SPECT images reconstructed using an iterative maximum-likelihood algorithm. *Phys Med Biol* 1994;38:1713–1726.
19. Blankespoor SC, Hasegawa BH, Brown JK, Heanue JA, Gould RG, Cann CE. Development of an emission-transmission CT system combining x-ray CT and SPECT. *Conf Rec IEEE Nucl Sci Symp Med Imag Conf* 1994;4:1758–1761.
20. Beyer T, Kinahan PE, Townsend DW, Sashin D. The use of x-ray CT for attenuation correction of PET data. *Conf Rec IEEE Nucl Sci Symp Med Imag Conf* 1994;4: 1573–1577.

Effects of Cilazapril and Verapamil on Myocardial Iodine-125-Metaiodobenzylguanidine Accumulation in Cardiomyopathic BIO 53.58 Hamsters

Yasushi Wakabayashi, Chinori Kurata, Tadashi Mikami, Sakae Shouda, Kenichi Okayama and Kei Tawarahara

Department of Medicine III, Hamamatsu University School of Medicine, Hamamatsu, Japan

Sympathetic nervous system activation is important in the pathophysiology of congestive heart failure. However, little about how the treatment for heart failure may influence myocardial sympathetic nervous activity has been established. In this study, we evaluated effects of cilazapril (CLZ) and verapamil (VER) on myocardial sympathetic nervous activity in cardiomyopathic BIO 53.58 hamsters using [^{125}I]metaiodobenzylguanidine ([^{125}I]MIBG). **Methods:** We used BIO 53.58 hamsters aged 3, 6 and 10 mo and age-matched normal F1b hamsters. We divided BIO 53.58 hamsters into untreated, CLZ- and VER-treated groups. We measured myocardial [^{125}I]MIBG uptakes and norepinephrine concentrations and evaluated the extent of fibrosis and the distribution of [^{125}I]MIBG. **Results:** The myocardial [^{125}I]MIBG uptake was significantly lower in BIO 53.58 hamsters aged 6 and 10 mo than in age-matched F1b hamsters. Myocardial [^{125}I]MIBG uptake was significantly correlated to myocardial norepinephrine concentration in BIO 53.58 hamsters. Myocardial [^{125}I]MIBG uptake was significantly higher in both of the treated groups than in the untreated group. The extent of myocardial fibrosis was significantly lower in both of the treated groups than in the untreated group. The myocardial [^{125}I]MIBG uptake showed a significant inverse correlation with the extent of fibrosis. Myocardial [^{125}I]MIBG distribution was highly heterogeneous in the untreated BIO 53.58 hamsters, whereas it was homogeneous in the F1b hamsters aged 6 mo and the treated BIO 53.58 hamsters. **Conclusion:** In BIO 53.58 hamsters, myocardial [^{125}I]MIBG uptake decreased with the progression of cardiomyopathy, and the decreased uptake was improved by treatment with CLZ and VER. Thus, myocardial [^{125}I]MIBG uptake can reflect the effects of treatment on cardiomyopathy, as well as the progression of cardiomyopathy.

Key Words: iodine-125I-MIBG; cardiomyopathy; angiotensin-converting enzyme inhibitor; calcium antagonist; sympathetic nervous activity

J Nucl Med 1997; 38:1540–1545

Activation of the sympathetic nervous system is important in the pathophysiology of congestive heart failure (*1*). The concentration of norepinephrine (NE) in the coronary sinus or myocardium and myocardial NE spillover have been determined as indices of the myocardial sympathetic nervous activity (*2–4*). These methods, however, were invasive and unsuitable

Received Mar. 12, 1996; revision accepted Aug. 12, 1996.

For correspondence or reprints contact: Yasushi Wakabayashi, MD, Division of Cardiology, Iwata Municipal Hospital, 57-1 Kounodai, Iwata 438 Japan.

TABLE 1
Findings of F1b and BIO 53.58 Hamsters in the First Study

	Body weight (g)		Heart/body weight ratio		Ascites and pleural effusion	
Age (mo)	F1b	BIO 53.58	F1b	BIO 53.58	Fib	BIO 53.58
3	114 ± 6	98 ± 7*	0.0034 ± 0.0003	0.0030 ± 0.0002*	0	0
6	126 ± 13	129 ± 10	0.0034 ± 0.0002	0.0029 ± 0.0001†	0	0
10	131 ± 14	135 ± 15	0.0036 ± 0.0002	0.0033 ± 0.0005	0	4

*$p < 0.01$ vs. F1b aged 3 mo.
†$p < 0.05$ vs. F1b aged 6 mo.

for widespread application or repeated measurement. Recently, it was shown that noninvasive scintigraphy with [^{123}I]metaiodobenzylguanidine ([^{123}I]MIBG), an analog of guanethidine that shares neuronal transport, storage and release mechanisms with NE, can image efferent adrenergic nerve terminals in the heart. This is known to reflect the myocardial sympathetic nervous activity (*5–7*).

The BIO 14.6 Syrian hamster develops a hereditary cardiomyopathy, terminating in congestive heart failure, and provides a good model for the experimental study of cardiomyopathy (*8–10*). The BIO 53.58 Syrian hamster is an inbred strain that arose as a spontaneous mutation of the BIO 14.6 strain (*11*). In contrast to the BIO 14.6 hamsters, the BIO 53.58 hamsters do not develop myolysis or hypertrophy before dilation, have a significantly shorter life span and demonstrate reduced cardiac function at an earlier age than do the BIO 14.6 hamsters (*12,13*). Therefore, the BIO 53.58 hamster provides a model of dilated cardiomyopathy that contrasts with a model of hypertrophic cardiomyopathy for the BIO 14.6 strain.

Angiotensin-converting enzyme inhibitors are used for the treatment of congestive heart failure as first-line drugs, and their effectiveness in reducing mortality and morbidity has been widely recognized (*14–16*). Cilazapril (CLZ), an angiotensin-converting enzyme inhibitor, has been reported to inhibit the progression of myocardial damages in cardiomyopathic Syrian hamsters (*17*). Furthermore, verapamil (VER), a calcium antagonist, has been reported to have a similar protective effect against cardiomyopathy (*18–20*).

The purposes of this study are to assess myocardial sympathetic nervous activities in the BIO 53.58 hamsters by using [^{125}I]MIBG and to investigate the question of whether the myocardial [^{125}I]MIBG uptake can detect the therapeutic effect of CLZ and VER on cardiomyopathy.

TABLE 2
Myocardial Iodine-125-MIBG Uptake and NE Concentration in the First Study

	[^{125}I]MIBG (% kg dose/g)		NE (μg/g)	
	F1b	BIO 53.58	F1b	BIO 53.58
3 mo	0.34 ± 0.05	0.35 ± 0.07	1.3 ± 0.5	1.7 ± 0.3
6 mo	0.42 ± 0.06*	0.23 ± 0.04†‡	1.9 ± 0.2	1.2 ± 0.2†‡
10 mo	0.40 ± 0.05*	0.23 ± 0.04†‡	1.9 ± 0.3	0.8 ± 0.3†‡§

*$p < 0.05$ vs. F1b aged 3 mo.
†$p < 0.01$ vs. BIO 53.58 aged 3 mo.
‡$p < 0.01$ vs. age-matched F1b.
§$p < 0.05$ vs. BIO 53.58 aged 6 mo.

MATERIALS AND METHODS

Animals

In the first study, male Syrian hamsters, aged 3, 6 and 10 mo, with dilated cardiomyopathy (BIO 53.58; Bio-Breeders, Inc., Fitchburg, MA; n = 10, 7 and 4, respectively) were used. Age-matched inbred male normal Syrian hamsters (F1b; n = 7, 7 and 7, respectively) served as controls.

In the second study, BIO 53.58 hamsters aged 3 mo were divided into the following three groups: an untreated group (n = 7), a CLZ-treated group (n = 7) and a VER-treated group (n = 7). CLZ (donated by Eizai Co. Ltd., Tokyo, Japan) was added to the drinking water, prepared fresh daily and given from ages 3 mo to 6 mo; the average intake was 1 mg/day (*17*). VER (donated by Eizai Co. Ltd., Tokyo, Japan) mixed with honey (to offset the bitter taste of VER) was added to the drinking water, prepared fresh daily and given from ages 3 mo to 6 mo; the average intake was 24 mg/day (*19*). Experiments on animals conformed to the Hamamatsu University School of Medicine regulations governing the care and use of laboratory animals.

MIBG Study

Iodine-125-MIBG had a specific activity of about 7.4 GBq/mg and a chemical purity of over 99%. In each animal group, [^{125}I]MIBG (3.7 MBq/kg) was injected via the femoral vein after anesthesia with intraperitoneal pentobarbital sodium. Four hours after the injection, the animals were killed under deep pentobarbital anesthesia. The hearts were removed, weighed and counted with an auto-well gamma counter. The myocardial [^{125}I]MIBG uptakes were expressed as percentage kilogram dose per gram (% kg dose/g).

After measurement of the myocardial [^{125}I]MIBG uptakes, the

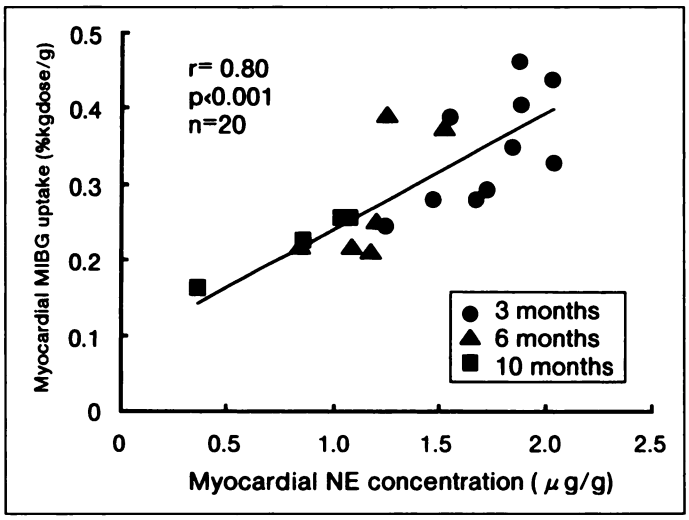

FIGURE 1. Relationship between myocardial [^{125}I]MIBG uptake and myocardial NE concentration in BIO 53.58 hamsters.

TABLE 3
Findings of BIO 53.58 Hamsters in the Second Study

Hamsters	Body weight (g)	Heart/body weight ratio	Ascites and pleural effusion
Untreated	129 ± 10	0.0029 ± 0.0001	0
CLZ-treated	110 ± 10*	0.0030 ± 0.0003†	0
VER-treated	96 ± 8*‡	0.0034 ± 0.0004†	0

*$p < 0.01$ vs. untreated.
†$p < 0.05$ vs. untreated.
‡$p < 0.05$ vs. CLZ-treated.

parts of the hearts were frozen in liquid nitrogen immediately. Then the myocardial NE concentration was measured by high-performance liquid chromatography. We measure the myocardial NE concentration in 4 F1b hamsters aged 3 mo, 4 F1b hamsters aged 6 mo, 5 F1b hamsters aged 10 mo, 10 BIO 53.58 hamsters aged 3 mo, 6 BIO 53.58 hamsters aged 6 mo and 4 BIO 53.58 hamsters aged 10 mo in the first study and in 6 BIO 53.58 hamsters aged 6 mo, 6 untreated hamsters, 6 CLZ-treated hamsters and 5 VER-treated hamsters in the second study.

Histological Study

The heart was sliced transversely at the midportion of the ventricle. Myocardial short-axis sections of 5 μm thickness were used for a histological evaluation in the second study. Masson's trichrome-stained specimens of myocardial sections were used for representation of fibrosis. The area of fibrosis was traced and calculated by an imaging analyzer system (*21*). The extent of fibrosis was evaluated with myocardial fibrosis ratio, which was defined as the percentage of the area of fibrosis in the whole myocardium. We measured the myocardial fibrosis ratio in six untreated BIO 53.58 hamsters, five CLZ-treated hamsters and four VER-treated hamsters.

Autoradiographical Study

We performed autoradiographical studies for the F1b hamsters aged 6 mo in the first study and for the three groups in the second study. After MIBG study, the hearts were frozen in liquid nitrogen and embedded in carboxylmethyl cellulose. The hearts were sliced transversely at the midportion of the ventricle using a cryomicrotome. Myocardial sections 20 μm in thickness were placed on x-ray films, and the autoradiographic exposure was performed for 100 days to obtain an adequate image quality.

To quantify myocardial distributions of [^{125}I]MIBG, a myocardial section was divided into five regions: the right ventricular wall, the right ventricular side of the interventricular septum, the left ventricular side of the interventricular septum, the endocardial region of the left ventricular free wall and the epicardial region of the left ventricular free wall. These selected regions of [^{125}I]MIBG autoradiograms were digitized and quantified using a digital image processing system. For each region, the relative uptake of the tracer was defined as the ratio of its optical density to the maximum optical density in the five regions. This relative uptake reflects the relative distribution of tracer in the myocardium. We measured the relative uptakes in four F1b hamsters aged 6 mo, four untreated BIO 53.58 hamsters, four VER-treated hamsters and five CLZ-treated hamsters.

TABLE 4
Myocardial Iodine-125-MIBG Uptake, NE and Fibrosis Ratio in the Second Study

Hamsters	[^{125}I]MIBG (% kg dose/g)	NE (μg/g)	Fibrosis ratio (%)
Untreated	0.23 ± 0.04	1.2 ± 0.2	35 ± 5
CLZ-treated	0.33 ± 0.08*	1.2 ± 0.6	18 ± 3†
VER-treated	0.47 ± 0.18†	0.9 ± 0.4	13 ± 4†

*$p < 0.05$ vs. untreated.
†$p < 0.01$ vs. untreated.

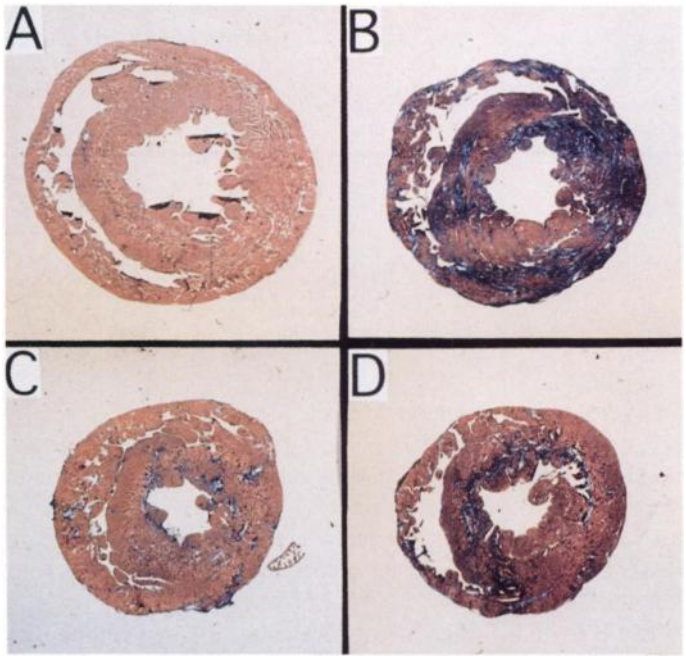

FIGURE 2. Masson's trichrome-stained specimens of myocardial sections in an F1b hamster aged 6 mo (A), an untreated BIO 53.58 hamster (B), a CLZ-treated BIO 53.58 hamster (C) and a VER-treated BIO 53.58 hamster (D). The extent of fibrosis is little in the F1b hamster aged 6 mo. The extent of fibrosis is significantly smaller in the CLZ- and VER-treated BIO 53.58 hamsters than in the untreated BIO 53.58 hamster.

Statistical Analysis

The mean data among the animal groups and myocardial regions were compared with ANOVA and Tukey's test. Associations between myocardial [^{125}I]MIBG uptake versus myocardial NE concentration and myocardial [^{125}I]MIBG uptake versus myocardial fibrosis ratio were studied with linear regression analysis. Data were expressed as mean ± s.d., and a probability of $p < 0.05$ was considered to be significant.

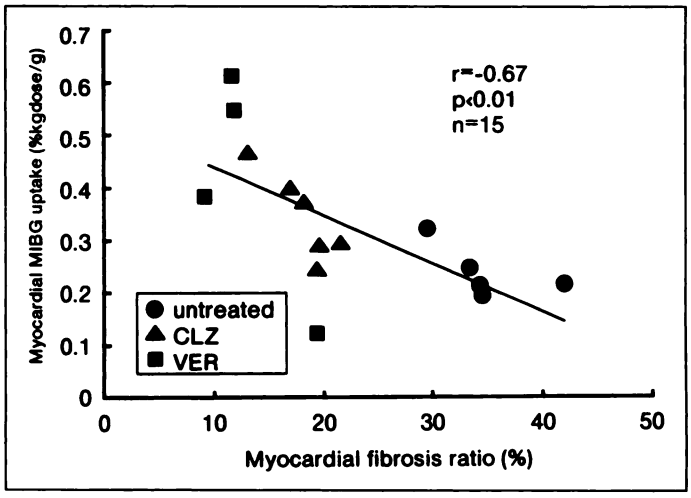

FIGURE 3. Relationship between myocardial [^{125}I]MIBG uptake and myocardial fibrosis ratio in untreated, CLZ-treated and VER-treated BIO 53.58 hamsters.

TABLE 5
Comparison of Relative Uptakes of Iodine-125-MIBG Between F1b Hamsters Aged 6 Mo and BIO 53.58 Hamsters in the Second Study

Groups	Regions				
	RV	SepR	SepL	LVend	LVepi
F1b (n = 4)	0.98 ± 0.01	0.98 ± 0.02	0.96 ± 0.04	0.96 ± 0.05	0.98 ± 0.01
Untreated (n = 4)	0.99 ± 0.01	0.98 ± 0.01	0.95 ± 0.02*	0.94 ± 0.02†‡	0.97 ± 0.02
CLZ-treated (n = 5)	0.98 ± 0.01	0.96 ± 0.02	0.94 ± 0.03	0.96 ± 0.02	0.97 ± 0.01
VER-treated (n = 4)	0.98 ± 0.01	0.97 ± 0.03	0.93 ± 0.05	0.95 ± 0.03	0.97 ± 0.02

*$p < 0.05$ vs. RV.
†$p < 0.01$ vs. RV.
‡$p < 0.05$ vs. SepR.
RV = right ventricular wall; SepR = right ventricular side of the interventricular septum; SepL = left ventricular side of the interventricular septum; LVend = endocardial region of the left ventricular free wall; LVepi = epicardial region of the left ventricular free wall.

RESULTS

Table 1 shows the findings of each group in the first study. The body weight was significantly lower in BIO 53.58 hamsters aged 3 mo than in age-matched F1b hamsters ($p < 0.01$). The body weight was not significantly different between BIO 53.58 hamsters aged 6 and 10 mo and age-matched F1b hamsters. The heart/body weight ratio was significantly lower in BIO 53.58 hamsters aged 3 and 6 mo than in age-matched F1b hamsters ($p < 0.01$). Pleural effusion and ascites were present only in BIO 53.58 hamsters aged 10 mo. They were absent in other groups.

Table 2 shows the myocardial [^{125}I]MIBG uptakes and NE concentrations of each group in the first study. The myocardial [^{125}I]MIBG uptake was not significantly different between BIO 53.58 and F1b hamsters aged 3 mo ($p > 0.05$). The myocardial [^{125}I]MIBG uptake was significantly lower in BIO 53.58 hamsters aged 6 and 10 mo than in age-matched F1b hamsters ($p < 0.01$). The myocardial [^{125}I]MIBG uptake was significantly higher in F1b hamsters aged 6 and 10 mo than in F1b hamsters aged 3 mo ($p < 0.05$). On the other hand, the myocardial [^{125}I]MIBG uptake was significantly lower in BIO 53.58 hamsters aged 6 and 10 mo than in BIO 53.58 hamsters aged 3 mo ($p < 0.01$).

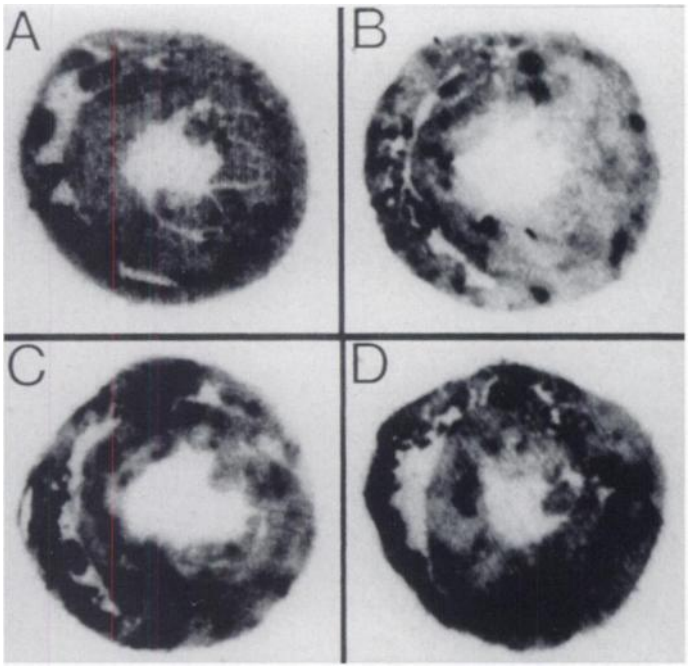

FIGURE 4. Illustrative digitized autoradiograms with [^{125}I]MIBG in an F1b hamster aged 6 mo (A), an untreated BIO 53.58 hamster (B), a CLZ-treated BIO 53.58 hamster (C) and a VER-treated BIO 53.58 hamster (D). The myocardial distribution of [^{125}I]MIBG is highly heterogeneous in the untreated BIO 53.58 hamster. On the other hand, the myocardial distribution of [^{125}I]MIBG is homogeneous in the F1b hamster aged 6 mo, the CLZ-treated hamster and the VER-treated BIO 53.58 hamster.

The myocardial NE concentration was not significantly different between BIO 53.58 and F1b hamsters aged 3 mo ($p = 0.09$). The myocardial NE concentration was significantly lower in BIO 53.58 hamsters aged 6 and 10 mo than in age-matched F1b hamsters ($p < 0.01$). The myocardial NE concentration was higher in F1b hamsters aged 6 and 10 mo than in F1b hamsters aged 3 mo ($p = 0.07$ and $p = 0.06$, respectively). The myocardial NE concentration was significantly lower in BIO 53.58 hamsters aged 6 and 10 mo than in BIO 53.58 hamsters aged 3 mo ($p < 0.01$). The myocardial NE concentration was significantly lower in BIO 53.58 aged 10 mo than in BIO 53.58 hamsters aged 6 mo ($p < 0.05$).

The relationship between myocardial [^{125}I]MIBG uptake and myocardial NE concentration in BIO 53.58 hamsters is shown in Figure 1. The myocardial [^{125}I]MIBG uptake was significantly correlated to myocardial NE concentration ($r = 0.80$; $p < 0.001$; $n = 20$).

Table 3 shows the findings of each group in the second study. The body weight was significantly lower in the CLZ- and VER-treated BIO 53.58 hamsters than in the untreated BIO 53.58 hamsters ($p < 0.01$). The heart/body weight ratio was significantly higher in the CLZ- and VER-treated BIO 53.58 hamsters than in the untreated BIO 53.58 hamsters ($p < 0.05$). Pleural effusion and ascites were absent in all groups.

Table 4 shows the myocardial [^{125}I]MIBG uptake, NE concentration and fibrosis ratio in the second study. The myocardial [^{125}I]MIBG uptake was significantly higher in the CLZ- and VER-treated BIO 53.58 hamsters than in the untreated BIO 53.58 hamsters ($p < 0.05$ and $p < 0.01$, respectively). On the other hand, the myocardial NE concentration was not different among these three groups ($p > 0.05$).

The myocardial fibrosis ratio was significantly lower in the CLZ- and VER-treated BIO 53.58 hamsters than in the untreated BIO 53.58 hamsters ($p < 0.01$; Table 4 and Fig. 2). The relationship between myocardial [^{125}I]MIBG uptake and myocardial fibrosis ratio is shown in Figure 3. The two variables showed a significant inverse correlation ($r = -0.67$; $p < 0.01$; $n = 15$).

As shown in Table 5, the relative uptakes of [^{125}I]MIBG did not differ among the five regions in F1b hamsters aged 6 mo ($p > 0.05$). On the other hand, in the untreated BIO 53.58 hamsters, the relative uptake of [^{125}I]MIBG was significantly

lower in the left ventricular side of the septum than in the right ventricular wall ($p < 0.05$) and was significantly lower in the endocardial region of the left ventricular free wall than in the right ventricular wall and right ventricular side of the septum ($p < 0.01$ and $p < 0.05$, respectively). In the CLZ- and the VER-treated BIO 53.58 hamsters, the relative uptakes of [^{125}I]MIBG did not differ among the five regions (Fig. 4).

DISCUSSION

The BIO 53.58 hamster develops a dilated, or congestive, form of cardiomyopathy characterized by thin ventricular walls and dilated chambers throughout most of its life (*12*). The myocardial [^{125}I]MIBG uptake in BIO 53.58 hamster decreased with aging, that is, the progression of dilated cardiomyopathy. Previous studies have shown enhanced early washout of [^{123}I]MIBG with reduced myocardial [^{123}I]MIBG uptake on delayed images in patients with dilated cardiomyopathy compared with normal healthy volunteers (*22–25*). Similar results were reported in a canine model of heart failure (*26,27*). The present report is the first description of changes in the myocardial [^{125}I]MIBG uptake with progression of dilated cardiomyopathy in an animal model.

A significant positive correlation was found between the myocardial NE concentration and the myocardial [^{125}I]MIBG uptake in BIO 53.58 hamsters. Previous studies have also shown a significant positive correlation between the myocardial NE content and the myocardial versus mediastinal [^{123}I]MIBG activity ratio in patients with dilated cardiomyopathy (*24*), as well as between the left ventricular tissue NE content and the [^{123}I]MIBG heart/lung ratio in a canine model of heart failure (*26*). The NE content was significantly greater in regions showing normal [^{123}I]MIBG compared with regions showing reduced [^{123}I]MIBG, confirming regional denervation in the dog heart (*28*). These results demonstrate that the decreased myocardial [^{123}I]MIBG uptake may reflect a depletion of NE from the myocardial sympathetic nerve terminals. The mechanisms for the reduction in [^{125}I]MIBG uptake and myocardial NE concentration in BIO 53.58 hamsters were not evaluated in this study. We can speculate that the decrease in myocardial NE concentration may be due to decreased neuronal uptake into sympathetic nerve terminals (*29,30*), increased turnover or release of NE from sympathetic nerve terminals (*31–33*) and decreased synthesis of NE in sympathetic nerves (*34*).

The treatments with CLZ and VER improved the myocardial [^{125}I]MIBG uptake and myocardial fibrosis ratio in BIO 53.58 hamsters. A previous report showed that chronic treatment with CLZ decreased cardiac angiotensin II levels and improved left ventricular performance in cardiomyopathic hamster (*17*). Another angiotensin-converting enzyme inhibitor, lisinopril, lowered cardiac adrenergic drive and increased a beta-receptor density in subjects with heart failure (*4*). Thus angiotensin-converting enzyme inhibitors may not only act on the systemic vasodilation but also directly inhibit the release of NE from the sympathetic nerve terminals (*4,35*). In addition, angiotensin-converting enzyme inhibitors may improve myocardial fibrosis by the inhibition of the tissue renin-angiotensin system (*36*). Previous reports showed that VER may improve cardiomyopathy by preventing calcium overload and microvascular spasm in the myocardium (*19,20*). In addition, VER may directly inhibit the release of NE from the sympathetic nerve terminals (*37*). Thus, both CLZ and VER may inhibit the overactivity of myocardial sympathetic nervous system, as well as the progression of myocardial fibrosis.

On the other hand, myocardial NE concentrations were not significantly improved by the treatments with CLZ and VER. Decrease in plasma NE concentration associated with improvement of heart failure by CLZ or VER may cause the discrepancy between myocardial NE concentration and [^{125}I]MIBG uptake in the CLZ- and the VER-treated BIO 53.58 hamsters, because the reduced plasma NE level may decrease NE content in synaptic clefts and increase [^{125}I]MIBG uptake in sympathetic nerve terminals. Any of the common effects of CLZ and VER, for example, the decrease of systemic blood pressure, may not improve the myocardial NE concentration and may not influence the myocardial MIBG uptake. These mechanisms are unknown. Furthermore, the discrepancy may be due to decreased NE synthesis in sympathetic nerves of BIO 53.58 hamsters (*33,34*). Further studies are needed to address this issue.

The myocardial distribution of [^{125}I]MIBG in the untreated BIO 53.58 hamsters was highly heterogeneous with significantly decreased uptake in the endocardial region of the left ventricular free wall and left ventricular side of the intraventricular septum. On the other hand, the myocardial distribution of [^{125}I]MIBG was homogeneous in F1b hamsters aged 6 mo and in the CLZ- and the VER-treated BIO 53.58 hamsters. We have already reported that the BIO 14.6 hamsters have more distinct regional heterogeneity in left ventricular distribution of [^{125}I]MIBG (*38*). Thus, the myocardial sympathetic innervation may be heterogeneous in cardiomyopathy. In this study, the treatment with CLZ and VER in BIO 53.58 hamsters improved the heterogeneity in myocardial [^{125}I]MIBG distribution, that is, in myocardial sympathetic innervation.

CONCLUSION

We have shown that the myocardial [^{125}I]MIBG uptake in BIO 53.58 hamsters decreased with aging, that is, the progression of dilated cardiomyopathy, the decreased [^{125}I]MIBG uptake and the heterogeneity of [^{125}I]MIBG distribution were improved by administrations of CLZ and VER in BIO 53.58 hamsters. Thus, myocardial [^{125}I]MIBG uptake can reflect the effects of treatment for cardiomyopathy, as well as the progression of cardiomyopathy.

REFERENCES

1. Thomas JA, Marks BH. Plasma norepinephrine in congestive heart failure. *Am J Cardiol* 1978;41:233–243.
2. Schofer J, Tews A, Langes K, Bleifeld W, Reimitz PE, Mathey DG. Relationship between myocardial norepinephrine content and left ventricular function: an endomyocardial biopsy study. *Eur Heart J* 1987;8:748–753.
3. Hasking GJ, Esler MD, Jennings GL, Burton D, Johns JA, Korner PI. Norepinephrine spillover to plasma in patients with congestive heart failure: evidence of increased overall and cardiorenal sympathetic nervous activity. *Circulation* 1986;73:615–621.
4. Gilbert EM, Sandoval A, Larrabee P, Renlund DG, O'Connell JB, Bristow MR. Lisinopril lowers cardiac adrenergic drive and increases β-receptor density in the failing human heart. *Circulation* 1993;88:472–480.
5. Sisson JC, Wieland DM, Sherman P, Mangner TJ, Tobes MC, Jacques S Jr. Metaiodobenzylguanidine as an index of the adrenergic nervous system integrity and function. *J Nucl Med* 1987;28:1620–1624.
6. Sisson JC, Shapiro B, Meyers L, et al. Metaiodobenzylguanidine to map scintigraphically the adrenergic nervous system in man. *J Nucl Med* 1987;28:1625–1636.
7. Wieland DM, Wu JL, Brown LE, Mangner TJ, Swanson DP, Beierwaltes WH. Radiolabeled adrenergic neuron-blocking agents: adrenomedullary imaging with iodine-125-iodobenzylguanidine. *J Nucl Med* 1980;21:349–353.
8. Homburger F, Baker JR, Nixon CW, Whitney R. Primary generalized polymyopathy and cardiac necrosis in an inbred line of Syrian hamsters. *Med Exp* 1962;6:339–345.
9. Bajusz E, Baker JR, Nixon CW, Homburger F. Spontaneous hereditary myocardial degeneration and congestive heart failure in a strain of Syrian hamsters. *Ann NY Acad Sci* 1969;156:105–129.
10. Bishop SP, Sole MJ, Tilley LP. Cardiomyopathies. In: Andrews EJ, Ward BC, Altman NH, eds. *Spontaneous models of human disease*. New York: Academic Press; 1979:59–64.
11. Feldman AM, Tena RG, Kessler PD, et al. Diminished β-adrenergic receptor responsiveness and cardiac dilation in hearts of myopathic Syrian hamsters (BIO 53.58) are associated with a functional abnormality of the G stimulatory protein. *Circulation* 1990;81:1341–1352.
12. Whitmer JT. L-Carnitine treatment improves cardiac performance and restores high-energy phosphate pools in cardiomyopathic Syrian hamster. *Circ Res* 1987;61:396–408.

13. Whitmer JT, Kumar P, Solaro RJ. Calcium transport properties of cardiac sarcoplasmic reticulum from cardiomyopathic Syrian hamsters (BIO 53.58 and 14.6): evidence for a quantitative defect in dilated myopathic hearts not evident in hypertrophic hearts. *Circ Res* 1988;62:81–85.
14. Packer M. Therapeutic options in the management of chronic heart failure. Is there a drug of first choice? *Circulation* 1989;79:198–204.
15. CONCENSUS Trial Study Group. Effects of enalapril of mortality in severe congestive heart failure. *N Engl J Med* 1987;316:1429–1435.
16. Pfeffer MA, Pfeffer JM, Steinberg C, Finn P. Survival after an experimental myocardial infarction: beneficial effects of long-term therapy with captoril. *Circulation* 1985;72:406–412.
17. Nakamura F, Nagano M, Kobayashi R, et al. Effects of an angiotensin-converting enzyme inhibitor, cilazapril, on congestive heart failure in cardiomyopathic hamsters. In: Nagano M, Takeda N, Dhalla NS, eds. *The cardiomyopathic heart*. New York: Raven Press: 1994:145–156.
18. Factor SM, Cho S, Scheuer J, Sonnenblick EH, Malhotra A. Prevention of hereditary cardiomyopathy in the Syrian hamster with chronic verapamil therapy. *J Am Coll Cardiol* 1988;12:1599–1604.
19. Wikman-Coffelt J, Sievers R, Parmley WW, Jasmin G. Verapamil preserves adenine nucleotide pool in cardiomyopathic Syrian hamster. *Am J Physiol* 1986;250:H22–H28.
20. Factor SM, Minase T, Cho S, Dominitz R, Sonnenblick EH. Microvascular spasm in the cardiomyopathic Syrian hamster: a preventable cause of focal myocardial necrosis. *Circulation* 1982;2:342–354.
21. Yamashita T, Kobayashi A, Yamazaki N, Miura K, Shirasawa H. Effects of L-carnitine and verapamil on myocardial carnitine concentration and histopathology of Syrian hamster BIO 14.6. *Cardiovasc Res* 1986;20:614–620.
22. Henderson EB, Kahn JK, Corbett JR, et al. Abnormal ^{123}I-metaiodobenzylguanidine myocardial washout and distribution may reflect myocardial adrenergic derangement in patients with congestive cardiomyopathy. *Circulation* 1988;78:1192–1199.
23. Glowniak JV, Turner FE, Gray LL, Palac RT, Lagunas-Solar MC, Woodward WR. Iodine-123-metaiodobenzylguanidine imaging of the heart in idiopathic congestive cardiomyopathy and cardiac transplants. *J Nucl Med* 1989;30:1182–1191.
24. Schofer J, Spielmann R, Schuchert A, Weber K, Schluter M. Iodine-123-metaiodobenzylguanidine scintigraphy: a noninvasive method to demonstrate myocardial adrenergic nervous system disintegrity in patients with idiopathic dilated cardiomyopathy. *J Am Coll Cardiol* 1988;12:1252–1258.
25. Merlet P, Dubois-Rande JL, Adnot S, et al. Myocardial β-adrenergic desensitization and neuronal norepinephrine uptake function in idiopathic dilated cardiomyopathy. *J Cardiovasc Pharmacol* 1992;19:10–16.
26. Simmons WW, Freeman MR, Grima EA, Hsia TW, Armstrong PW. Abnormalities of cardiac sympathetic function in pacing-induced heart failure as assessed by [^{123}I]metaiodobenzylguanidine scintigraphy. *Circulation* 1994;89:2843–2851.
27. Rabinovitch MA, Rose CP, Rouleau JL, et al. Iodine-123-metaiodobenzylguanidine scintigraphy detects impaired myocardial sympathetic neuronal transport function of canine mechanical-overload heart failure. *Circ Res* 1987;61:797–804.
28. Dae MW, O'Connell JW, Botvinick EH, et al. Scintigraphic assessment of regional cardiac adrenergic innervation. *Circulation* 1989;79:634–644.
29. Rose CP, Burgess JH, Cousineau D. Tracer norepinephrine kinetics in coronary circulation of patients with heart failure secondary to chronic pressure and volume overload. *J Clin Invest* 1985;76:1740–1747.
30. Liang CS, Fan TH, Sullebarger JT, Sakamoto S. Decreased adrenergic neuronal uptake activity in experimental right heart failure. A chamber-specific contributor to beta-adrenoceptor down-regulation. *J Clin Invest* 1989;84:1267–1275.
31. Meredith IT, Eisenhofer G, Lambert GW, Dewar EM, Jennings GL, Esler MD. Cardiac sympathetic nervous activity in congestive heart failure: evidence for increased neuronal norepinephrine release and preserved neuronal uptake. *Circulation* 1993;88:136–145.
32. Sole MJ, Lo C, Laird CW, Sonnenblick EH, Wurtman RJ. Norepinephrine turnover in the heart and spleen of the cardiomyopathic Syrian hamster. *Circ Res* 1975;37:855–862.
33. Sole MJ, Helke CJ, Jacobowitz DM. Increased dopamine in the failing hamster heart: transvesicular transport of dopamine limits the rate of norepinephrine synthesis. *Am J Cardiol* 1982;49:1682–1690.
34. Pool PE, Covell JW, Levitt M, Gibb J, Braunwald E. Reduction of cardiac tyrosine hydroxylase activity in experimental congestive heart failure. *Circ Res* 1967;20:349–353.
35. Minato H, Hosoki K, Sawayama T, Kadokawa T, Hashimoto M. Antihypertensive mechanism of alacepril. Effects of its metabolites on the peripheral sympathetic nervous system. *Arzneim-Forsch/Drug Res* 1989;39:319–324.
36. Sawa H, Kawaguchi H, Mochizuki N, et al. Distribution of angiotensinogen in diseased human heart. *Mol Cell Biochem* 1994;132:15–23.
37. Jaques S, Tobes MC, Sisson JC. Effect of calcium channel blockers on acetylcholine stimulated and basal release of metaiodobenzylguanidine and norepinephrine in cultured bovine adrenomedullary cells. *J Nucl Med* 1987;28:639–640.
38. Taguchi T, Kobayashi A, Kurata C, Tawarahara K, Yamazaki N. Dual-tracer autoradiography with thallium-201 and iodine-125 MIBG in BIO 14.6 cardiomyopathic Syrian hamsters. *Jpn Circ J* 1993;57:1089–1096.